**Award Number: 01HQGR0118**


**SURFACE-TO-BEDROCK, SHEAR-WAVE AND GEOTECHNICAL INVESTIGATION OF THE MISSISSIPPI EMBAYMENT BETWEEN THE 35$^{TH}$ AND 36$^{TH}$ PARALLELS: COLLABORATIVE RESEARCH WITH THE UNIVERSITY OF KENTUCKY AND UNIVERSITY OF MEMPHIS**

Ron Street
University of Kentucky
Kentucky Geological Survey
Lexington, Kentucky 40506-0107

Telephone: (859) 257-5500
Fax: (859) 257-1147
Email: none

Edward Woolery
University of Kentucky
Department of Geological Sciences
Lexington, Kentucky 40506-0053

Telephone: (859) 257-5500
Fax: (859) 323-1938
Email: woolery@uky.edu

**Program Element: II**

**SURFACE-TO-BEDROCK, SHEAR-WAVE AND GEOTECHNICAL INVESTIGATION OF THE MISSISSIPPI EMBAYMENT BETWEEN THE 35TH AND 36TH PARALLELS: COLLABORATIVE RESEARCH WITH THE UNIVERSITY OF KENTUCKY AND UNIVERSITY OF MEMPHIS**

Ron Street
University of Kentucky
Kentucky Geological Survey
Lexington, Kentucky 40506-0053
Telephone: (859) 257-5500
Fax: (859) 257-1147
Email: none

Edward Woolery
University of Kentucky
Department of Geological Sciences
Lexington, Kentucky 40506-0053
Telephone: (859) 257-3016
Fax: (859) 323-1938
Email: woolery@uky.edu

## ABSTRACT

A P- and S-wave velocity model of the post-Paleozoic sediments has been developed across the Upper Mississippi Embayment between the latitudes of 35¼ and 35½°N. The model was constructed by P-wave soundings and reversed SH-wave refraction/reflection profiles acquired at 5-km intervals along the corridor. The results from these data were integrated with previously acquired P- and SH-wave velocity estimates, P-wave CDP reflection profiles, P-wave sonic logs, travel-time differences between earthquake-generated S- and S$p$-waves, and top of bedrock elevation from nearby drillholes. A three-layered S-wave velocity model is proposed from this dataset. The uppermost layer, which is not discussed in this paper (see Street *et al*., 2001), varies from a few tens of meters thick near the edges of the embayment to as much as 190 m near the center of the study area; the S-wave velocities of these unlithified to poorly lithified sediments are highly variable (typically ranging between 150 and 600 m/s) and site-dependent. The second layer in the S-wave velocity model extends from the base of the near-surface layer to the acoustical top of the Cretaceous sediments, which is ~650 m below sea level near the center of the study area. The lateral S-wave velocity variance of this layer is defined in three segments: 1) near the western edge of the study area in northeastern Arkansas the velocity varies between 650 and 700 m/s, 2) the central study area ranges between 795 and 840 m/s, and 3) near the eastern edge of the study area in western Tennessee between 500 and 550 m/s. The S-wave velocities of the third layer, the Cretaceous section, vary between 725 and 775 m/s at the edges of the study area, but ranges between 1,010 and 1,060 m/s near the center.

## INTRODUCTION AND OBJECTIVES

As described by Toro *et al.* (1992), the Upper Mississippi Embayment is a large wedge-shaped syncline that dips to the south, and is filled with several tens to several hundreds of meters of unlithified and semi-lithified, post-Paleozoic sediments (Figure 1). Underlying the embayment, and aligned approximately with its axis is the New Madrid seismic zone, which Cramer (2001) estimated is capable of producing large (> M7) earthquakes at mean-recurrence intervals of 498 years. The effects of the unlithified embayment sediments on ground motions from a damaging earthquake are poorly understood because of the lack of instrumental records, and a lack of reliable *S*-wave velocity data for the deeper (> 100 m) sediments. The sediments in the embayment, as well as the subsurface bedrock topography, could have a significant effect on the earthquake ground motions in the area. *S*-waves propagating upward through thick layers of unlithified sediments are apt to be amplified and induce resonance at selected frequencies. Resonance can also be set up in a sediment-filled basin if the *S*-waves are incident to the edge of the basin, and the width of the basin is comparable to its depth (Frankel, 1994).

*P*- and *SH*-wave seismic reflection and refraction data have been acquired at 57 sites (Figure 2). The 57 sites were chosen for a reasonable spatial distribution, proximity to drillholes that penetrated into bedrock, and proximity to seismograph stations from which earthquake travel-time differences between the direct *S*- and top-of-bedrock converted *Sp*-waves are known. In addition, existing drillhole data, *P*- and *SH*-wave seismic reflection/refraction data, and earthquake travel-time differences between the direct *S*- and top-of-bedrock converted *Sp*-waves were used to estimate the *S*-wave velocities of sediments across the study area.

## ESTIMATING SEISMIC VELOCITIES

A fundamental problem in seismic exploration is the uncertainty in estimating velocity. Consequently, depths derived from seismic data are never entirely reliable (Yilmaz, 1987). In order to minimize the uncertainty, information from well logs, proprietary and published P-wave seismic reflection profiles, travel times of seismic waves from earthquakes, and near-surface (<100 m) S-wave velocity-depth profiles were used to constrain the velocity interpretations. Other useful results from related studies in the area are summarized below.

### Geology and Depth to Bedrock

Figure 3a shows the physiographic provinces and generalized cross section of the post-Paleozoic sediments in the study area. The Western Lowlands and St. Francis Basins are flat-lying floodplains dominated by sluggish streams, meander belts, buried stream channels, and clayey silts. Separating the basins is Crowleys Ridge, a north-south feature that on the average is elevated 60 m above the basin floors. The ridge is composed of Eocene and Pliocene-Pleistocene unlithified fluvial sands, gravels, and clays (Saucier, 1974). The ridge has been shown by VanArsdale *et al.* (1992) to have a structural origin.

East of the St. Francis Basin are the West Tennessee Plain and the West Tennessee Upland (Stearns, 1975). As indicated in Figure 3a, the western half of the West Tennessee Plain is covered with a thin layer of Pleistocene loess. Going eastward across the West Tennessee

Upland, the soils sequentially change from Eocene sand, to Paleocene clay and sand, to Cretaceous sand and marl.

The surficial soils in the study area, though not discussed in this paper because of the highly site-specific nature (see Street *et al.*, 2001), are important. NEHRP building code provisions (BSSC, 1997) classify sites and assign amplification factors on the basis of the time-averaged S-wave velocities of the upper 30 m of sediment; moreover, the liquefaction potential at a site is strongly influenced by the depth to the water table, layering, and composition of these uppermost sediments. Furthermore, because surficial soils tend to have relatively low S-wave velocities, their presence has a significant impact on the overall average S-wave velocity of post-Paleozoic sediments – a factor which, in our opinion, is best accounted for by a site-specific geotechnical ground-motion evaluation.

The lower boundary of our model is the top of the Paleozoic bedrock, which is characterized by a sharp increase in the S- and P-wave velocities. The depth to the Paleozoic bedrock in the study area is known from drillhole data compiled by Dart (1992). Figure 3b shows the locations of the wells in the study area that Dart (1992) listed as having reached or penetrated the top of the Paleozoic bedrock. Also included in Figure 3b is that part of the contoured bedrock surface (datum is msl) shown in Wheeler et al. (1994).

*P-Wave CDP Seismic Lines*
In addition to the existing drillhole and depth-to-rock data, the seismic velocities and depths to the bedrock in this study are constrained by existing P-wave CDP lines, travel times of earthquake arrivals at nearby seismograph stations, and our P- and SH-wave reflection and refraction surveys. Figure 4 shows the locations of the existing P-wave CDP seismic reflection lines, seismograph stations, and the sites where our P- and SH-wave reflection and refraction data were acquired. The seismic-reflection lines, shown as solid lines in the figure, have been published, whereas those shown as dashed lines are unpublished proprietary lines. Note the shot-point interval for seismic lines C, L, and P is 220 ft (67.7 m). Although this interval is generally adequate for imaging the top of the Cretaceous and Paleozoic horizons, it is too large to be considered high-resolution for any horizon. The shotpoint interval for seismic line MSF was 10 m. Seismic line MSF was acquired to image structure within the post-Paleozoic sediments, and reflections were correlated with the stratigraphic information of nearby well logs (Williams *et al.*, 2001).

The seismic lines shown in Figure 4 are a small sample of the several hundred kilometers of proprietary Vibroseis P-wave reflection profiles acquired in the Upper Mississippi Embayment during the late 1970's and early 1980's. Clearly seen in most of these profiles, as well as the shorter, higher-resolution seismic lines (e.g., those described in Sexton et al., 1982; Luzietti et al., 1992; Woolery et al., 1996, 1999; and Williams et al., 2001) are tops of the Cretaceous (K) sediments and Paleozoic bedrock (Pz). Based on the seismic sections from the published and proprietary seismic lines, the tops of the Cretaceous and Paleozoic surfaces are expected to appear relatively smooth with a gentle dip toward the center of the study area.

*Stratigraphy, Seismic Reflectors, and P-Wave Velocities*
The post-Paleozoic stratigraphy, P-wave reflector coherency, and seismo-stratigraphic
correlations are well established in the St. Francis Basin. Figure 5, modified from Luzietti et al.
(1992), shows the generalized stratigraphy for the area. Included in the figure are the P-wave
reflection horizons used by Luzietti et al. (1992, 1995) to interpret the P-wave seismic lines BS-4
and GL-5 (not shown), and by Williams et al. (2001) in interpreting P-wave seismic line MSF
(Figure 4).

The P-wave CDP seismic-reflection profiles, drill logs/stratigraphic column, P-wave root-mean-
square (RMS), and interval velocities were used to estimate the characteristics of the post-
Paleozoic sediments in this part of the study area (Fig. 3a). The P-wave velocities derived in
previous studies were relatively consistent in the area. For example, Crone (1992) estimated the
RMS P-wave stacking velocity to be 1,951 m/s to the top of the Cretaceous section, and 2,134
m/s to the top of the Paleozoic bedrock. Williams et al. (2001) concluded from seismic line MSF
(Figure 4) that the average P-wave velocity of the sediments ranged between 1,600 m/s at a
depth of 200 m and approximately 2,000 m/s at the top of the Cretaceous. Luzietti et al. (1992)
estimated that the P-wave interval velocity of the Cretaceous section was 2,335 m/s. In addition
to the surface-derived P-wave velocity estimates, a P-wave sonic log from the Houston Oil
Mineral/No. 1 Singer hole (i.e., AR5 in Dart, 1992) was incorporated into the study. The sonic
log from the hole and a section of the P-wave sounding acquired nearby (site 26) are shown in
Figure 6. The locations of the drillhole and site 26 are approximately 800 m apart (Figure 3).
The resulting RMS P-wave velocity to the top of the Paleozoic at site 26 is 1,975 m/s (Figure 6).

*Earthquake Data*
Three 3-component seismograph stations are located in the study area (Figure 4). Differences in
the arrival times of earthquake phases at the stations can be used to estimate the average S-wave
velocity of the post-Paleozoic sediments at the station sites. Andrews et al. (1985) noted that a
secondary wave, the S-to-P (S$p$) wave, is often observed on the vertical traces of seismograms
for seismic stations in the New Madrid seismic zone. They identified this wave as a converted
wave generated at the base of the post-Paleozoic sediments. Chiu et al. (1992) and Chen et al.
(1996) used the travel-time differences between the S$p$-wave on the vertical trace and the S-wave
on the horizontal traces of three-component seismograms to estimate the average S-wave
velocity ($V_s$) of the sediments. They related the difference in travel times, $d(t_s - t_{Sp})$, to the
thickness of the sediments (H) and the average P-wave velocity ($V_p$) at the site by the equation
$$d(t_s - t_{Sp}) \sim H/V_s - H/V_p \qquad (1)$$
where time is in seconds, and depth and velocities are in m and m/s, respectively. Because the
depth to bedrock is known (Figure 3b), and $V_p$ of the sediments at the station sites were
determined in this study (see discussion below), $V_s$, the average S-wave velocity, of the
sediments at the three seismic stations were determined using equation 1.

*Other Criteria Used in Estimating Seismic Velocities*
The published and the proprietary P-wave CDP seismic lines suggest the stacking and interval
velocities for the deeper (>100 m) unlithified sediments in the Upper Mississippi Embayment
change gradually with lateral distance (i.e., not more than a few tens of m/s over distances of
several tens of kilometers. Consequently, P-wave RMS and interval velocities acquired in this

study at sites that averaged 5 km in separation were interpreted with the expectation they would vary only slightly between sites.

At sites where SH-wave data were acquired, SH-wave refraction and reflections were generally recorded.  In such cases, intercept times obtained from the reflection data were compared to the travel time of a vertically propagating S-wave in the refraction model.

*Summary*
Several sets of data and criteria were used to constrain seismic velocity interpretations.  The depths to the bedrock at the selected sites are reasonably well known (Wheeler et al., 1994).  Furthermore, the velocities of the P-waves in the Cretaceous section are known to be significantly greater than in the overlying sediments, and the seismic stratigraphy (P-wave) near the center of the study area are well established from the studies of Luzietti et al. (1995) and Williams et al. (2001), as well as the sonic log for the Houston Oil Minerals/No. 1 Singer drillhole.  In addition, the travel-time differences between the S- and Sp-waves at three seismograph stations have been determined near the central study area.  The stations are separated by approximately 10 km.  Travel-time differences in converted waves were used to estimate the average S-wave velocities of the sediments at the station sites.

**ACQUISITION AND PROCESSING OF THE SEISMIC DATA**
Two sets of seismic data were acquired at the 57 sites investigated (Figure 2): P-wave reflection soundings to the top of the Paleozoic bedrock, and reversed SH-wave refraction/reflection profiles (used to determine the S-wave velocities of the unlithfied sediments to depths as great as 160 m).  The energy sources used for P-wave data acquisition were a seismic hammer and vacuum-assisted weight drop.  The receivers were inline spreads of twenty-four or forty-eight 40-Hz vertical component geophones spaced at intervals of 4 m or 6.1 m.  The seismic hammer was used at sites where the depth to bedrock was less than 100 m.  At some of the sites in western Tennessee this included determining the depth to the water table.  The weight drop was used at all sites where the depth to bedrock exceeded 100 m.  The seismic hammer was used at the 0-m source offset position, whereas the weight drop was used at stepped-out offsets of one to four times the length of the geophone spread, as well as the zero offset, depending upon the length of the geophone spread, the quality of the recorded signal, and the depth to bedrock.  In general, we used 48 geophones spaced at 6.1 m, and stepouts of 0 and 292.6 m with the weight-drop source. The inline-offset panels were combined to form a P-wave section representing the range of source-receiver offsets.  Figure 7a shows traces 46 through 95 of a 96-channel P-wave sounding acquired at site 28.

The P-wave section in Figure 7a is typical of the data collected in the study area, except for five sites (sites 22 through 26) on and adjacent to Crowleys Ridge (Figure 2) where Cretaceous reflections were weak.  The poor quality of the seismic data at these sites is thought to be the result of drought conditions at the time the data were collected.  Because of the dry surficial soils, the geophones were coupled poorly to the ground.  Also, much of the energy of the weight drop was dissipated in the dry near-surface soils.

SH-wave data were acquired using a seismic hammer striking an I-beam in the manner described in Street et al. (1995). Inline spreads of twenty-four or forty-eight 30-Hz horizontally polarized geophones, spaced at intervals of 4 m or 6.1 m, were used. The seismic hammer was used at the 0-m offset positions at both ends of the geophone spreads. Figure 8a shows the SH-wave data acquired at site 28; the quality is typical of the SH-data collected during this study. The P- and SH-wave field files were processed on PC's using the commercial software package VISTA7.0 (Seismic Image Software Ltd., 1996). Typical processing consisted of converting the raw files into SEG-Y format files, bandpass filtering, applying an automatic gain control (AGC), and using a frequency-wave number (FK) filter to remove residual ground roll. Timing corrections due to changes in elevation between the shotpoint and geophones were not included in the processing because the seismic profiles were acquired at sites with little or no relief. Various bandpass filters, AGC windows, and FK filters were applied to the data. This was necessary because of depth variations, and the field conditions encountered (i.e., highway traffic, irrigation pumps, soil types, etc.).

The two-way intercept times and stacking velocities from interpreted P- and SH-waves were estimated using an interactive hyperbolic curve-fitting computer algorithm for the $X^2$-$T^2$ analysis. Interval velocities were calculated using Dix's (1955) equation. An example (site 28) of this P-wave velocity-depth interpretation process is shown in Figure 7.

First-break arrival times for the refracted SH-waves were interpreted by the seismic-refraction software package SIPT2 v.4.1 (Rimrock Geophysics, Inc., 1995) to derive S-wave velocity-depth models. SIPT2 uses the delay-time method to obtain a first approximation of the velocity-depth model by comparing the observed first-break picks to those computed using ray tracing. The model is then iteratively adjusted to decrease the travel-time differences between the first-break picks and model-calculated arrival times based on the model. The S-wave velocity-depth model for site 27, based on the reversed seismic-refraction modeling, is shown in Figure 8(b).

**_P_- AND _S_-WAVE VELOCITIES OF THE POST-PALEOZOIC SEDIMENTS**
Figure 9 shows the P- and S-wave velocity model derived in this study for the post-Paleozoic sediments across the Upper Mississippi Embayment at ~35¼ to 35½ ° latitude. As previously noted, depths to reflectors derived from seismic data are not entirely reliable because of the uncertainty in estimating velocity from such data. These uncertainties arise from the lack of moveout in the reflection over the length of the geophone spread being used, the inherent resolution limitations, and the lack of a signal at various distances caused by interference from coherent noise and/or a low reflection coefficient (due to the angle of incidence). The P- and S-wave velocity models in Figure 9 are based on the P-wave soundings and SH-wave refraction/reflection profiles acquired during this study, the velocity and drillhole data from the aforementioned studies, and the d(ts - tS$p$) travel times at the three nearby seismograph stations. The P- and S-wave velocities for the Paleozoic bedrock are 5,000 and 3,000 m/s, respectively (Williams et al., 2002).

*P-Wave Velocities*
RMS velocities to the top of the Fort Pillow (Paf), Cretaceous (K), and Paleozoic (Pz) horizons were interpreted from the P-wave soundings across the study area. Figures 10a through 10c show the P-wave RMS velocities plotted as a function of the acquisition location. The dashed lines in the plots are the least- squares fit to the velocity estimates. Because the drillhole data indicated gently dipping horizons that vary only slightly with lateral distances, the least-squares-fitted RMS velocities represent the preferred estimates. RMS velocities of the sediments near the center of the embayment are greater than the RMS velocities of the sediments near the edges of the embayment because the higher velocity sediments are thicker in the center, and the sediments in the center are, in general, more consolidated and stiff as a result of the greater depth of burial.

Crone's (1992) study of the Crittenden County fault zone between 90¼° and 90½° W used 2,134 m/s for the RMS P-wave velocity to the top of the bedrock, which agrees reasonably well with our RMS velocity estimates (Figure 10c). The reflections and RMS P-wave velocities corresponding to the tops of the Fort Pillow Formation and the Cretaceous section (Figure 10) were correlated with seismic lines BS-4, GL-2, L, and MSF (Figure 4). As previously mentioned, Crone (1992) and Williams et al. (2001) estimated the RMS velocities to the top of the Cretaceous in their respective study areas as 1,951 and 2,000 m/s. These estimates (Figure 10b) correspond with our best-fit dashed results for the Cretaceous RMS P-wave velocity.

The P-wave velocities for the Cretaceous and the sediments between sea level and the top of the Cretaceous (Figure 9a) are based on: (1) interval velocities using Dix's (1955) equation at sites in this study, (2) the P-wave sonic logs for the Upper Mississippi Embayment shown in Gao et al. (in review), and (3) velocity estimates from previous studies in the area by others. The average P-wave velocity of the Cretaceous sections from the sonic logs in Gao et al. (in review) is 2,301 m/s, and the average P-wave velocity of the sediments from the top of the Memphis Sand to the top of the Cretaceous section (Figure 4) is 1,970 m/s. The velocity analysis chart of Hamilton and Zoback (1982) for seismic line D yields an RMS P-wave velocity of approximately 1,980 to the top of the Cretaceous, and a Cretaceous P-wave interval velocity of approximately 2,370 m/s.

The material properties of the uppermost sediment layer (i.e., those sediments down to a depth of approximately 100 m) are highly variable. Contributing to the variability in the velocities of the sediments are geomorphic factors such as depositional environment (e.g., fluvial or aeolian), depositional features (e.g., buried stream channels), and the depth of the water table. In general, the P-wave velocities of the uppermost layer were found to vary between approximately 900 m/s for loose, unsaturated sediments, and 1,800 m/s for denser, stiffer sediments.

*S-Wave Velocities*
The S-wave velocities shown in Figure 9b are based on direct observations of reflected and refracted SH- and P-waves for sites near the edges of the embayment, as well as a combination of near-surface refracted and reflected SH-waves, P-wave reflections, travel-time differences between S$p$- and S-waves from earthquakes, and empirical P- to S-wave velocity ratios for sites near the center of the study area.

For sites near the edges of the embayment, such as site 10 (Figure 2), we acquired reversed SH-wave refraction/reflection and P-wave reflection data. The near-surface S-wave velocities at the site were determined from the interpretation of the first-arrival times in the reversed SH-wave profiles. SH- and P-wave reflections were used to model the velocity structure of the sediments from the base of the SIPT2 model to the top of the bedrock. Figure 11a shows one side of the reversed SH-wave profile used in the refraction modeling. The three columns in Figures 11b through 11d show the S-wave velocities of the near-surface sediments at the site based on the SH-wave refraction model, as well as the S- and P-wave RMS and interval velocities (reflection data). The three velocity models in Figures 11b through 11d are consistent. The S-wave reflection at 27 m in column 2 agrees with the refraction velocity boundary at 26 m, and the RMS velocity of the upper layer in column 2 correlates with the time-averaged velocities of the refracted layers above 26 m in column 1. The P-wave reflections at 33, 182, and 223 m in column 3 correspond to the SH-wave interpretations in column 2 at 27, 173, and 220 m, respectively. The depths to bedrock derived from the SH- and P-wave data, 220 and 223 m, respectively, are supported by nearby drillhole data.

In the center of the study area, the post-Paleozoic sediments are several hundreds of meters thick, and a seismic hammer does not generate sufficient SH-wave energy to sample the entire sediment column down to the top of the bedrock; however, the seismograph stations TWAR, BLAR, and NFAR are nearby (Fig. 4). The travel-time differences between the earthquake-generated S- and Sp-waves, the depth to the top of the bedrock, and the P-wave velocities of the sediments at these stations are known. Therefore, equation 1 can be used to estimate the average S-wave velocities of the sediments at the seismograph stations.

Figure 12 outlines the procedure used for estimating the S-wave velocities of the post-Paleozoic sediments at the three seismograph stations. In Figure 12a, the thickness of the sediments, H, is derived from the depth-to-bedrock shown in Wheeler et al. (1994) and the elevations at the stations. $V_p$ is the P-wave velocity at the stations based on the least-squares fit of P-wave RMS velocities to the depth of bedrock (i.e., Figure 10c). $V_s$ and T are the S-wave velocities of the sediments using equation 1, and the travel times for a vertically propagating S-wave from the top of the bedrock to the surface. Figure 12b shows the near-surface S-wave velocities of the sediments for the seismograph stations in accordance with the reversed SH-wave refraction/reflection profiles. The deepest SH-wave reflection for seismic station NFAR is estimated to be for a horizon at 89 m. Based on our experience in collecting SH-wave data for this study, as well as experience gained in an earlier study (Street et al., 2001), it is likely that there is an intermediate velocity layer of 650 to 750 m/s at NFAR that was not detected in the SH-wave reflection record below 89 m.

Figure 12c gives the information used in estimating the S-wave velocities of the sediments at the station sites between the base of the S-wave velocity columns (as indicated in Figure 12b) and the top of the Paleozoic bedrock. t is the travel time of a vertically propagating S-wave (shown in the velocity columns in Figure 12b). $K^T$, the thickness of the Cretaceous sections at the seismograph stations, was derived from our P-wave reflection data. The S-wave velocities, $V_s$, shown for layer 2 (i.e., from the base of the soil columns as given in Figure 12b to the top of the Cretaceous section) and layer 3 (i.e., Cretaceous section) were derived by assuming that the S-

wave velocities of layer 3 are 218 m/s greater than the S-wave velocities in the Cretaceous section. The 218 m/s difference in the shear-wave velocities is based on the average of the differences (i.e., 218 ±37 m/s) in the SH-wave velocities between the Cretaceous section and the overlying sediments at seven sites along the edges of the basin.

Figure 12d shows the range of S-wave velocities estimated for layer 2 and the Cretaceous section at the three seismic stations. The shaded areas indicate the range of S-wave velocity values that are inclusive to all three stations, and represent the range of S-wave velocities shown in Figure 9b for layer 2 and the Cretaceous section, near the center of the figure.

## DISCUSSION
*Comparison to Previously Derived P- and S-Wave Velocity Models*
We have used a combination of P-wave soundings and CDP seismic-reflection bedrock profiles, near-surface (typically < 150 m) reversed SH-wave refraction and reflection profiles, drillhole elevation data, $d(t_s - t_{Sp})$ earthquake times, and observed velocity differences between the Cretaceous and overlying sediments to estimate the P- and S-wave velocities of the post-Paleozoic sediments. Other S-wave velocity models of the post-Paleozoic sediments in the Upper Mississippi Embayment have been published. For example, Toro et al. (1992) used the P-wave sonic log from the New Madrid Test Well 1-X described by Crone (1981), and a Poisson's ratio of 0.45 to estimate the S-wave velocity of the sediments. Dorman and Smalley (1994) used the P-wave sonic log from the Amoco Haynes well (i.e., AR99 in Dart, 1992), a modified form of Nafe and Drake's (1957) measurements of P- and S-wave velocities and expressions of bulk properties in clastic sediments, to derive an S-wave velocity model of the sediments. Chiu et al. (1992) and Chen et al. (1996) used the travel-time differences between the direct S- and S*p*-waves, depths to the top of the Paleozoic bedrock, and the P-wave velocity of 1.8 km/s given by Andrews et al. (1985) to estimate the S-wave velocities at seismic stations throughout the New Madrid seismic zone. Bodin and Horton (1999) and Bodin et al. (2001) measured the horizontal-vertical power spectral ratios (H/VPSR) of ambient microtremors in the range of 0.03 to 25 Hz, to determine the predominant period ($T_o$) of the sediments' vibrational resonance at a series of sites across the Upper Mississippi Embayment (along a line passing through Memphis, Tenn). They assumed that $T_o$ is related to the sediment thickness, H, and that the S-wave velocity, Vs, is given by the equation:

$$T_o = 4H/V_s. \tag{2}$$

From equation 2, Bodin *et al.* (2001) concluded:

$$V_s = 521.5 + 0.37459H \quad (350 < H < 1,100 \text{ m}). \tag{3}$$

Figure 13 compares the S-wave velocity models of Chiu et al. (1992), Toro et al. (1992), Dorman and Smalley (1994), and Bodin et al. (2001) to our derived S-wave velocity model for the seismograph station TWAR. The S-wave velocity model for Bodin et al. (2001) is based on equation 3 and an H of 900 m. As shown in Figure 13, our results most closely resemble those of Dorman and Smalley (1994).

Figure 14 compares the P-wave velocities of the post-Paleozoic sediments for the Houston Oil Minerals/No. 1 Singer, Amoco Haynes, and New Madrid Test Well 1-X (Figure 1). The P-wave

velocities of the sediments in these wells, as well as our P-wave soundings, suggest that the P-wave velocities in the Upper Mississippi Embayment sediments can be best modeled as consisting of three layers: an upper layer 100 to 150 m thick throughout the Embayment (excluding sites near the edges), an intermediate layer extending from the bottom of the upper layer to the Cretaceous sediment, and a bottom layer corresponding to the Cretaceous section. P-wave velocities in the top layer generally increase with depth, but are highly variable, and are often a function of the water table and degree of saturation. P-wave velocities in the intermediate layer tend to be relatively uniform, whereas P-wave velocities in the bottom layer can generally be subdivided into two layers: an upper layer corresponding to the Porters Creek Formation (Paleocene), and a lower, but higher velocity, layer corresponding to the McNairy Formation (Figure 5).

Based on the varying P-wave reflection amplitudes, the P-wave velocities in the upper and lower sections of layer 3 for the three wells (Figure 14), and our soundings, the P-wave velocities of the Cretaceous sediments show considerable variation over distances of several tens of kilometers. This is despite the fact that the RMS velocities to the top of layer 3 and the top of bedrock (Figures 10 b and 10c) tend to be predictable.

The P-wave velocities for the three layers in the proposed model also vary as a function of the depth of burial. This is physically reasonable, and is also supported by the P-wave soundings and a comparison of the P-wave velocities (Fig. 14) to the cross-hole and uphole velocity measurements of the P-wave velocities from the holes drilled for the vertical accelerometer array near the northern edge of the Embayment (Street et al. 1997).

Based on the new S-wave velocity data, as well as data from other studies (e.g., Street et al., 2001; Williams et al., 2003), the derived S-wave velocity models shown in Figure 13 suggest that S-wave velocities of the Upper Mississippi Embayment are, like the P-wave velocities, best represented by a three-layer velocity model. As with the P-wave velocity model, the uppermost layer consists of 100 to 150 m of sediments characterized by highly variable (vertically and laterally) S-wave velocities that generally increase as a function of depth. Between the bottom of the upper layer and the top of the Cretaceous horizon is an intermediate layer of relatively uniform S-wave velocities that can be considered a constant over distances of several tens of kilometers.

The bottom layer in the proposed S-wave velocity model corresponds to the Cretaceous section, and consists of two S-wave velocity layers that most likely differ by several tens to perhaps as much as 100+ m/s. This assertion is based on the velocity profile for the vertical accelerometer array at the northern edge of the Upper Mississippi Embayment (Street et al. 1997), and the other S-wave velocity models along the edge of the embayment (Street et al., 1997). Although we lack direct evidence of the S-wave velocities for individual sedimentary sequences at sites where the thickness of the sediments exceed 150 m, the idea that there are considerable differences in the S-wave velocities between the upper and lower Cretaceous sections corresponds with the P-wave velocities in this study, as well as the velocity models suggested by Toro et al. (1992) and Dorman and Smalley (1994) for the Upper Mississippi Embayment (Figure 13).

*Implications with Respect to Site-Specific Studies*
The primary result of this study has been the development of an S-wave velocity model across the Upper Mississippi Embayment near the southern terminus of the New Madrid seismic zone. Although often times overlooked, the presence of unlithified sediments in deep sedimentary basins can significantly influence site effects. It is well known, for example, that long-period surface waves generated by the conversion of body waves at the edge of a deep sedimentary basin can significantly contribute to the ground motions at sites in the basin. The presence of a thick layer of sediments will also affect the ground motions at a site by differentially attenuating the higher frequencies more so than the lower frequencies, thus setting up the potential for long-period basin resonances. In addition to the impedance contrast at the bedrock/sediment boundary, impedance boundaries within the unlithified sediments themselves can result in converted phases and resonances. In general, the overall effect of these phenomena is to dampen the peak ground motions because of the dampening of the higher frequencies, and to increase the duration of the strong-motions because of the converted phases and resonances.

The results of this study do not address the issue of attenuation in the sediments of the Upper Mississippi Embayment, but they do lend themselves to predicting three-dimensional basin resonances, and one-dimensional analyses. The results also suggest a methodology for estimating site-specific effects where detailed information is needed for critical structures. Based on our experience in acquiring SH- and P-wave seismic reflection/refraction data in the Upper Mississippi Embayment (Street et al., 1995, 1997b, 2001; Woolery et al., 1993, 1996, 1999), it relatively inexpensive to acquire seismic data to a depth of 100 to 150 m, which is the top the S-wave velocity model in this study. The site-specific seismic data would be used to define the velocities, the velocity structures (i.e., dipping beds, buried river channels, etc.), and the depth of the water table. Integrated with geotechnical testing, results from additional near-surface seismic measurements and the S- and P-wave models in this study (along with an assumed attenuation model for the unlithified sediments) can provide a rigorous basis for estimating the site-specific effects.

**CONCLUSIONS**
The objective of this study was to determine the S-wave velocity structure of the sediments between the top of the Paleozoic bedrock and the near-surface (<100 m) sediments across the Upper Mississippi Embayment between the latitude of 35¼ and 35½° N. This was accomplished by acquisition of P-wave soundings and reversed SH-wave reflection/refraction near-surface profiles at sites along this transect. The results of these data were used in conjunction with existing drillhole data, sonic logs, $d(t_s - t_{Sp})$ times generated by earthquakes, previously acquired near-surface SH-wave velocity profiles, and stratigraphic-seismic velocity correlations to develop a vertically and laterally varying S- and P-wave velocity model for sediments deeper than 100 m.

At the center of the study area, along the Arkansas-Tennessee border, the average sediment S-wave velocities from a depth corresponding to sea level to the acoustical top of the Cretaceous sediment (~650 m below sea level) are 785 to 840 m/s, whereas the Cretaceous sediments are 1,010 to 1,060 m/s. Away from the center of the embayment, the S-wave velocities decrease to

725 to 775 m/s for the Cretaceous material.  The overlying sediments range between 650 and 700 m/s in northeastern Arkansas, and between 500 and 550 m/s in western Tennessee.

## REFERENCES CITED

Andrews, M.C., W.D. Mooney, and R.P. Meyer (1985).  The relocation of microearthquakes in the Northern Mississippi Embayment, *J. Geophys. Res.* 90, 10223-10236.

Bodin, P., and S. Horton (1999).  Broadband microtremor observation of basin resonance in the Mississippi Embayment, central US, *Geophy. Res. Lett.* 26, 903-906.

Bodin, P., K. Smith, S. Horton, and H. Hwang (2001).  Microtremor observations of deep sediment resonances in metropolitan Memphis, Tennessee, *Eng. Geology* 62, 159-168.

Chen, K.-C., J.-M. Chiu, and Y.T. Yang (1996).  Shear-wave velocity of the sedimentary basin in the Upper Mississippi Embayment using *S*-to-*P* converted waves, *Bull. Seism. Soc. Am.* 86, 848-856.

Chiu, J.-M., A.C. Johnston, and Y.T. Yang (1992).  Imaging the active faults of the central New Madrid seismic zone using PANDA array data, *Seism. Res. Lett.* 63, 375-393.

Cramer, C.H. (2001).  A seismic hazard uncertainty analysis for the New Madrid seismic zone, *Eng. Geology* 62, 251-266.

Crone, A.J. (1981).  Sample description and stratigraphic correlation of the New Madrid test well 1-X, New Madrid County, Missouri, *U.S. Geol. Surv. Open-File Rept.* 81-426, 28 p.

Crone, A.J. (1992).  Structural relations and earthquake hazards of the Crittenden County Fault Zone, northeastern Arkansas, *Seism. Res. Lett.* 63, 249-262.

Dart, R.L. (1992).  Catalog of pre-Cretaceous drillhole data from the Upper Mississippi Embayment: A revision and update of Open-File Report 90-260, *U.S. Geol. Surv. Open-File Rept.* 90-685, 263 p.

Dix, C.H. (1955).  Seismic velocities from surface measurements, *Geophysics* 20, 68-86.

Dorman, J., and R. Smalley (1994).  Low-frequency seismic surface waves in the Upper Mississippi Embayment,  *Seism. Res. Lett.* 65, 137-148.

Frankel, A. (1994).  New developments in estimating basin response effects on ground motions, Proceedings of Seminar on New Developments in Earthquake Ground Motion Estimation and Implications for Engineering Design Practice, *Applied Technology Council, ATC* 35-1, 11-1-11-6.

Gao, F.C., J.M. Chiu, E. Schweig, and R. Street (in review). Three-dimensional *P*- and *S*-wave velocity structure in the sedimentary basin of the Upper Mississippi Embayment.

 Hamilton, R.M., and M.D. Zoback (1982). Tectonic features of the New Madrid seismic zone from seismic reflection profiles, in *Investigations of the New Madrid, Missouri, Earthquake Region*, edited by F.A. McKeown and L.C. Pakiser, *U.S. Geol. Surv. Prof. Papaer* 1236-F, 55-82.

Luzietti, E.A., L.R. Kanter, E.S. Schweig, K.M. Shedlock, and R.B. VanArsdale (1992). Shallow deformation along the Crittenden County Fault Zone near the southeastern margin of the Reelfoot Rift, northeast Arkansas, *Seism. Res. Lett.* 63, 263-275.

Luzietti, E.A., L.R. Kanter, E.S. Schweig, K.M. Shedlock, and R.B. VanArsdale (1995). Shallow deformation along the Crittenden County Fault Zone near the southeastern margin of the Reelfoot Rift, northern Arkansas, in *Investigations of the New Madrid Seismic Zone*, edited by K.M. Shedlock and A.C. Johnston, *U.S. Geol. Surv. Prof. Paper* 1538-J, J1-J23.

Nafe, J.E., and C.L. Drake (1957). Variation with depth in shallow and deep water marine sediments of porosity, density and the velocities of compressional and shear waves, *Geophysics* 22, 523-522.

Ng, K.W., T.S. Chang, and H. Hwang (1989). Subsurface conditions of Memphis and Shelby County, National Center for Earthquake Engineering Research, State University of New York at Buffalo, Buffalo, N.Y., *Technical Report NCEER-89-0021*.

Ni, S.-D., R.V. Siddharthan, and J.G. Anderson (1997). Characteristics of nonlinear response of deep saturated soil deposits, *Bull. Seism. Soc. Am.* 87, 342-355.

Rhea, S., and R.L. Wheeler (1994). Map showing locations of geophysical survey and modeling lines in the vicinity of New Madrid, Missouri, *U.S. Geol. Surv. Miscellaneous Field Studies Map MF-2264-C*, scale 1:250,000.

Rimrock Geophysics, Inc. (1995). SIPT2 Version 4.1 (and other programs), 56 p.

Saucier, R.T. (1974). Quaternary geology of the Lower Mississippi Valley, *Arkansas Archaeological Survey Research Series* 6, 26 p.

Seismic Image Software Ltd. (1996). VISTA 7.0 Notes, 477 p.

Sexton, J.L., E.P. Frey, and D. Malicki (1982). High-resolution seismic-reflection surveying on Reelfoot Scarp, northwestern Tennessee, in *Investigations of the NewMadrid, Missouri, Earthquake Region*, edited by F.A. McKeown and L.C. Pakiser, *U.S. Geol. Surv. Prof. Paper* 1236-J, 137-149.

Stearns, R.G. (1975). Field trips in west Tennessee, *Tennessee Division of Geology, Report of Investigations* 36, 4-7.

Street, R., Z. Wang, E. Woolery, J. Hunt, and J. Harris (1997). Site effects at a vertical accelerometer array near Paducah, Kentucky, *Eng. Geology* 46 (3-4), 349-367.

Street, R., E.W. Woolery, Z. Wang, and J.B. Harris (1995). A short note on shear-wave velocities and other site conditions at selected strong-motion stations in the New Madrid seismic zone, *Seism. Res. Lett.* 66, 56-63.

Street, R., E. Woolery, Z. Wang, and J. Harris (2001). NEHRP soil classifications for estimating site-dependent seismic coefficients in the Upper Mississippi Embayment, *Eng. Geology* 62, 123-135.

Toro, G.R., W.J. Silva, R.K. McGuire, and R.B. Herrmann (1992). Probabilistic seismic hazard mapping of the Mississippi Embayment, *Seism. Res. Lett.* 63, 449-475.

VanArsdale, R.B., E.S. Schweig, L.R. Kanter, R.A. Williams, K.M. Shedlock, and K.W. King (1992). Preliminary shallow seismic reflection survey of Crowleys Ridge, northeast Arkansas, *Seism. Res. Lett.* 63, 309-320.

Wheeler, R.L., S. Rhea, and R.L. Dart (1994). Map showing structure of the Mississippi Valley Graben in the vicinity of New Madrid, Missouri, *U.S. Geol. Surv. Miscellaneous Field Studies Map MF-2264-D*, scale 1:250,000.

Williams, R.A., W.J. Stephenson, J.K. Odum, and D.M. Worley (2001). Seismic-reflection imaging of Tertiary and related post-Eocene deformation 20 km north of Memphis, Tennessee, *Eng. Geology* 62, 79-90.

Williams, R.A., S. Wood, W.J. Stephenson, J.K. Odum, M.E. Meremonte, R. Street, and D.M. Worley (2003). Surface seismic-refraction/reflection measurements of Potential Site Resonances and the Areal Uniformity of NEHRP Site Class D in Memphis, Tennessee, *Earthquake Spectra*, v. 19, p. 159–189.

Woolery, E.W., and R. Street (2002). Near-surface soil response from H/V ambient noise ratios, *J. of Soil Dynamics and Earthquake Engineering*, 22, 865-876.

Woolery, E.W., R. Street, Z. Wang, J.B. Harris, and J. McIntyre (1999). Neotectonic structure in the central New Madrid seismic zone: Evidence from multimode seismic-reflection data, *Seism. Res. Lett.* 70, 554-576.

Woolery, E.W., Z. Wang, R. Street, and J.B. Harris (1996). A *P*- and *SH*-wave seismic reflection investigation of the Kentucky Bend Scarp in the New Madrid seismic zone, *Seism. Res. Lett.* 67, 67-74.

Yilmaz, O. (1987).  *Seismic Data Processing*, Society of Exploration Geophysicists, Investigations in Geophysics, Volume 2, Tulsa, Oklahoma, 526 p.
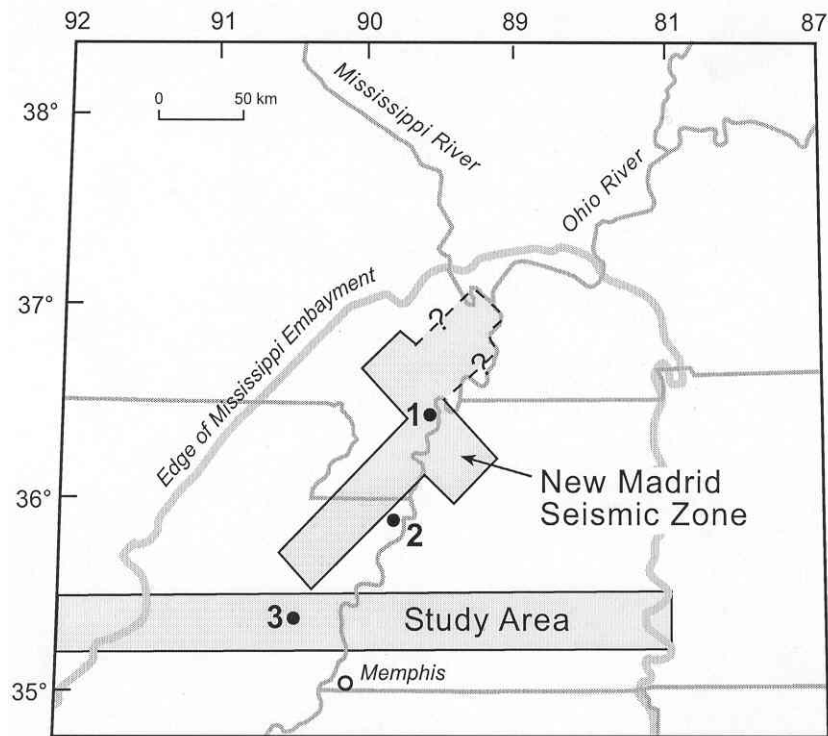
Figure 1. The Upper Mississippi Embayment, location of the New Madrid seismic zone, and the study area. Also shown are the locations of the New Madrid Test Well 1-X (1), the Amoco Haynes well (2), and the Houston Oil Minerals/No. 1 Singer well (3), which are discussed in the latter part of the text.
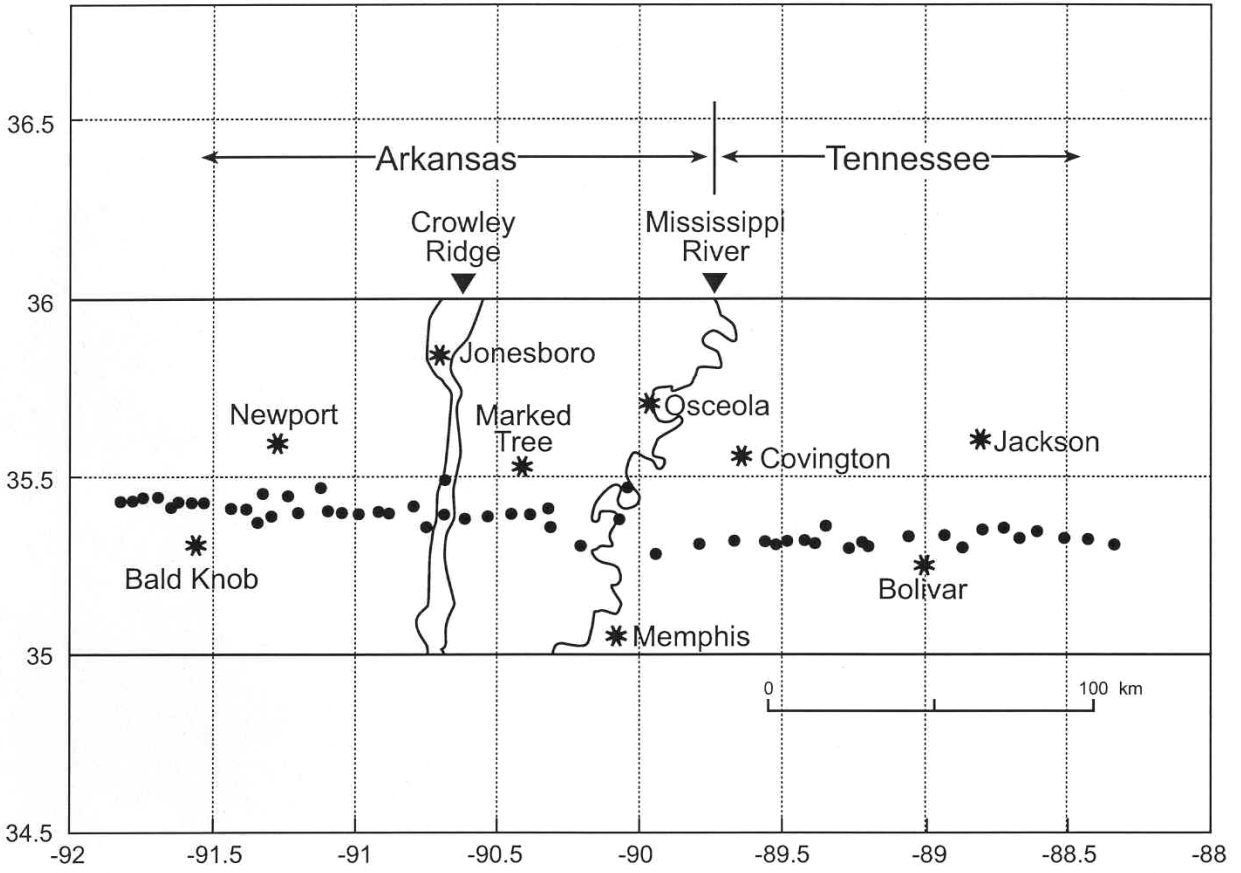
Figure 2. Site locations for the 57 P- and SH-wave seismic reflection and refraction surveys. Sites are numbered consecutively from west to east; for clarity, the site numbers are not shown.
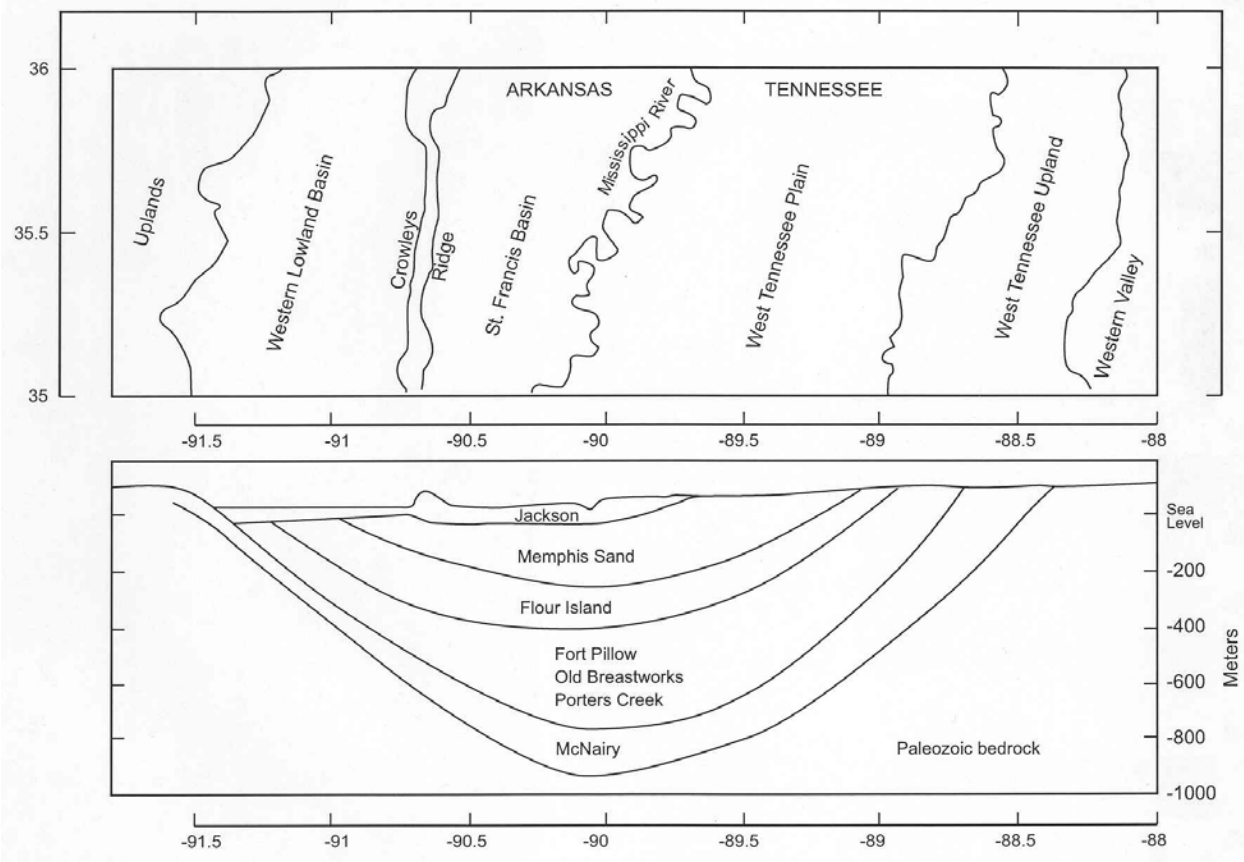
Figure 3a. A map of physiographic provinces, as well as a generalized cross section (not to scale) of the post-Paleozoic sediments (modified from Saucier, 1974; Stearns, 1975; and Ng et al., 1989).
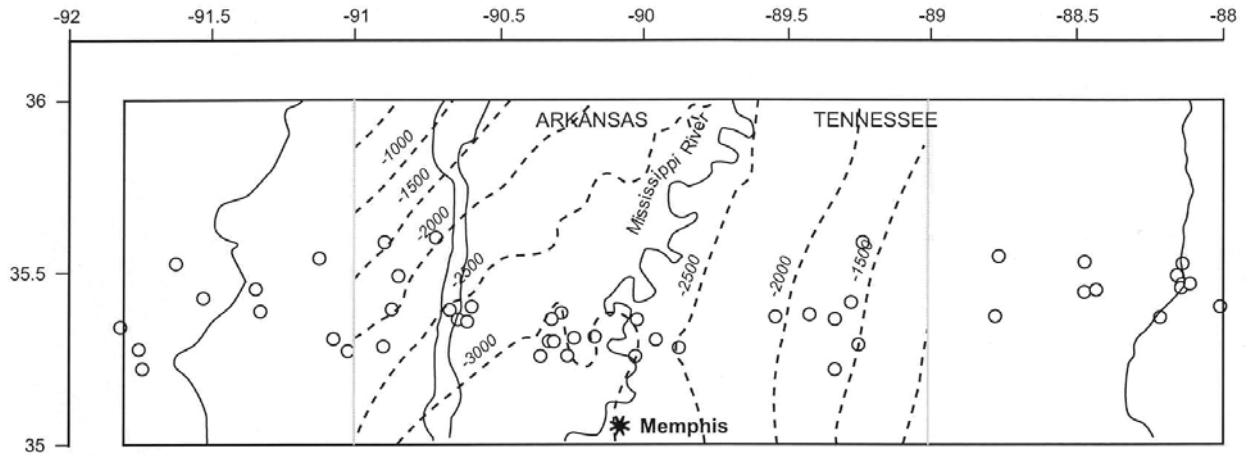
Figure 3b. Drillhole locations (open circles) in the study area that penetrate the top of Paleozoic bedrock (from Dart, 1992). The dashed lines in the center of the figure give the depth to the top of the Paleozoic bedrock (in feet) with respect to mean sea level (taken from Wheeler et al. (1994). The depth to the top-of-bedrock east and west of the contours shallows uniformly to the edges of the study area, where it outcrops.
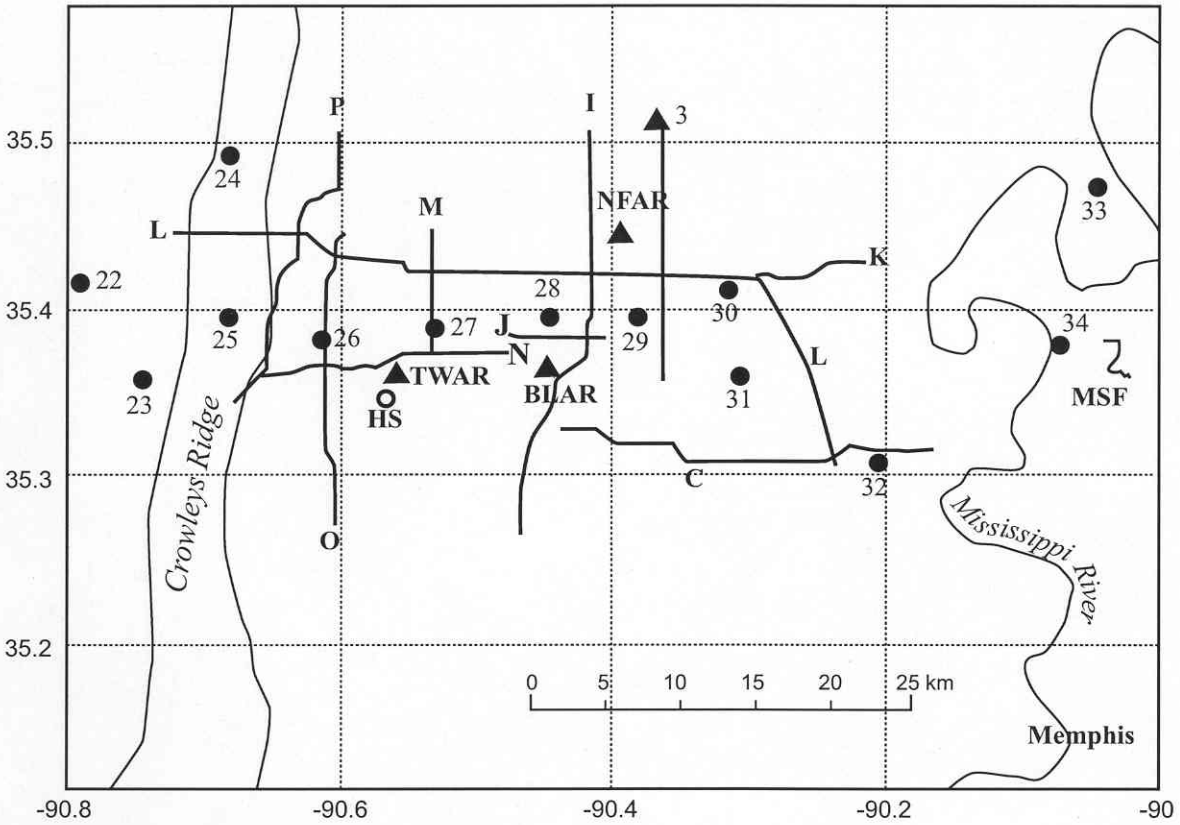
Figure 4. P-wave CDP seismic-reflection lines and seismic stations located in the study area, as well as the location of the Houston Oil Minerals/ No. 1 Singer (HS) drillhole. Locations and identification (i.e., I, J, K, etc.) of the seismic lines are taken from Rhea and Wheeler (1994), with the exception of line MSF, which is from Williams et al. (2001). Numbered sites (filled circles) are our survey locations, and correspond to those shown in Figure 2. Seismic stations BLAR, NFAR, and TWAR are operated and maintained by the University of Memphis.

21
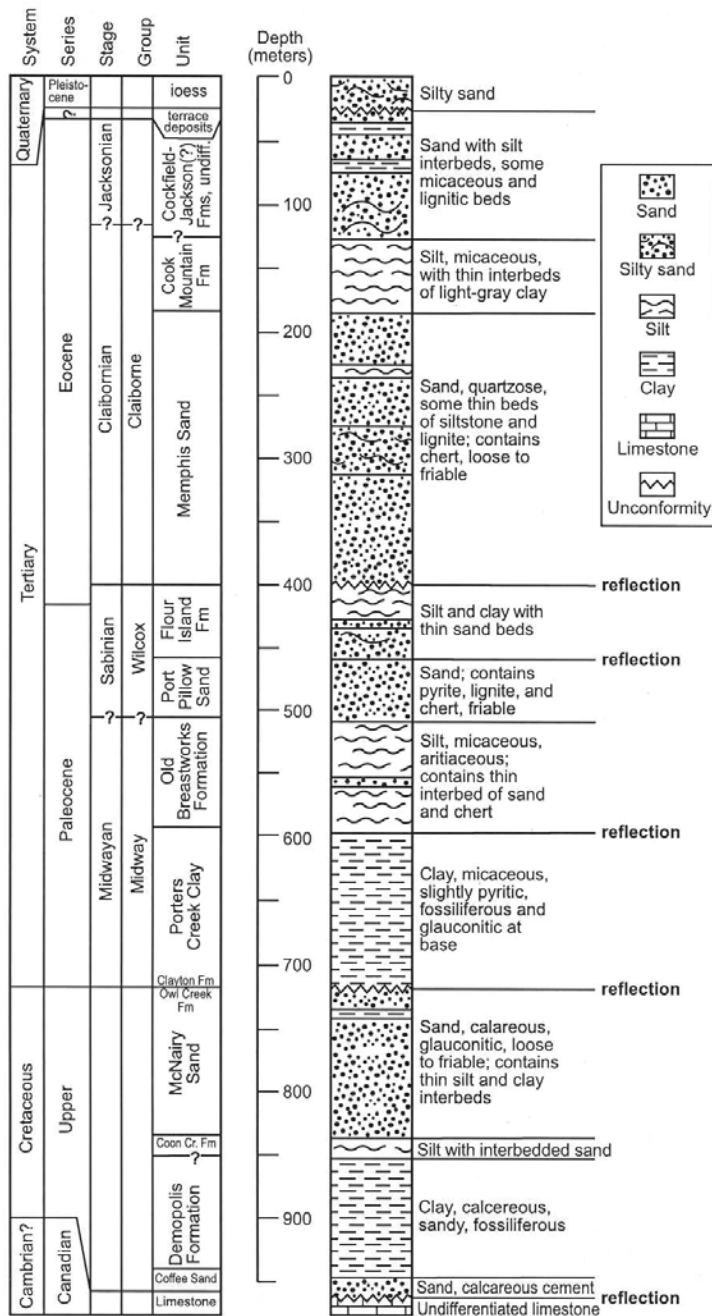
Figure 5. Stratigraphic column (from Luzietti et al., 1995) used for correlating our P-wave reflections with the geologic units. The emphasis was on determining the RMS velocities and depths to the top of the Fort Pillow (Paf), top of the Cretaceous (K), and top of the Paleozoic bedrock (Pz). Other reflections were frequently seen in the seismic sections (e.g., top of the Flour Island), but could not be correlated across the entire area.
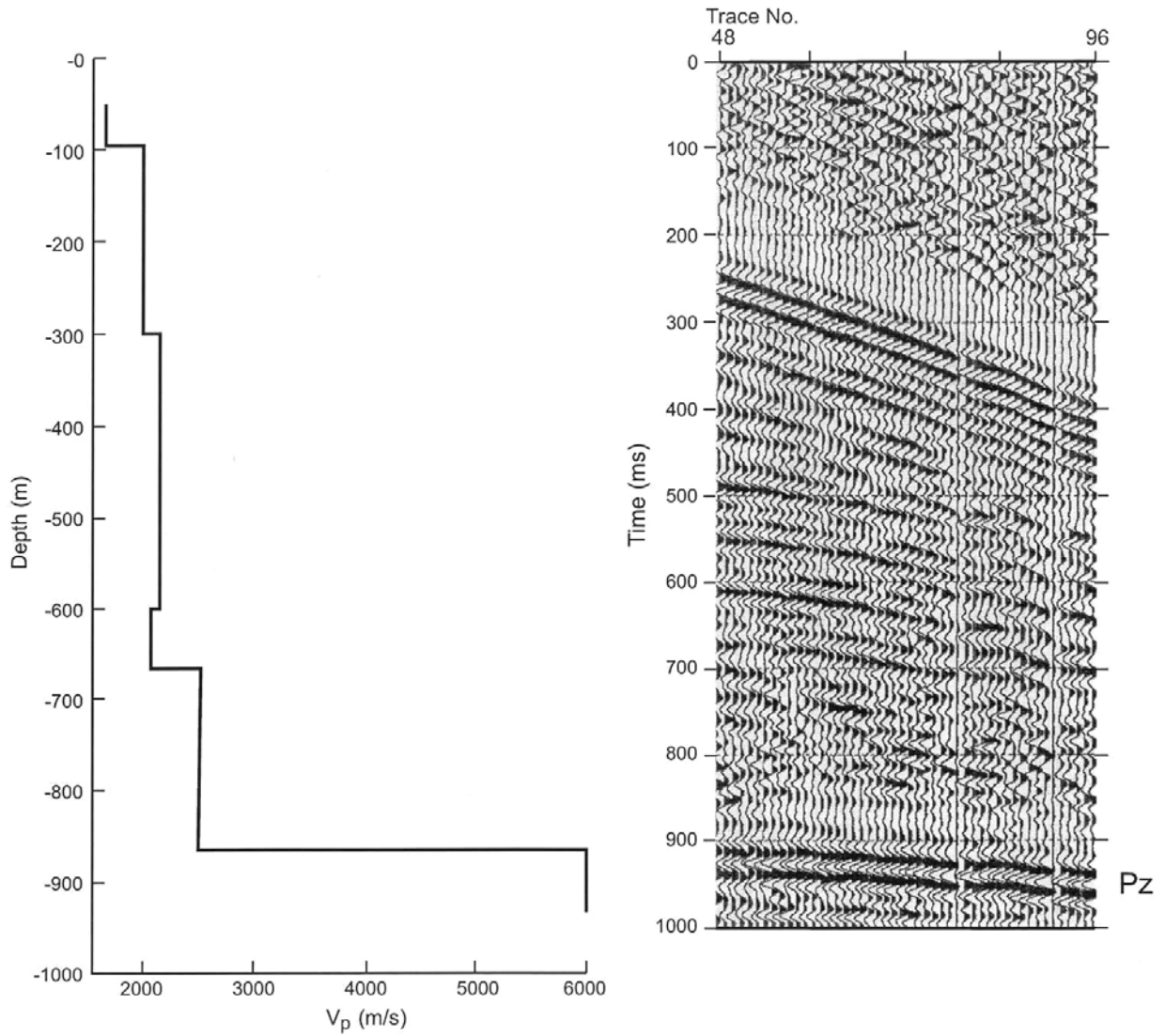
Figure 6. Sonic log for (a) the Houston Oil Minerals/ No. 1 Singer drillhole, and (b) P-wave seismic reflection sounding panel acquired at site 26 that shows the coherent top-of- bedrock reflection.

23
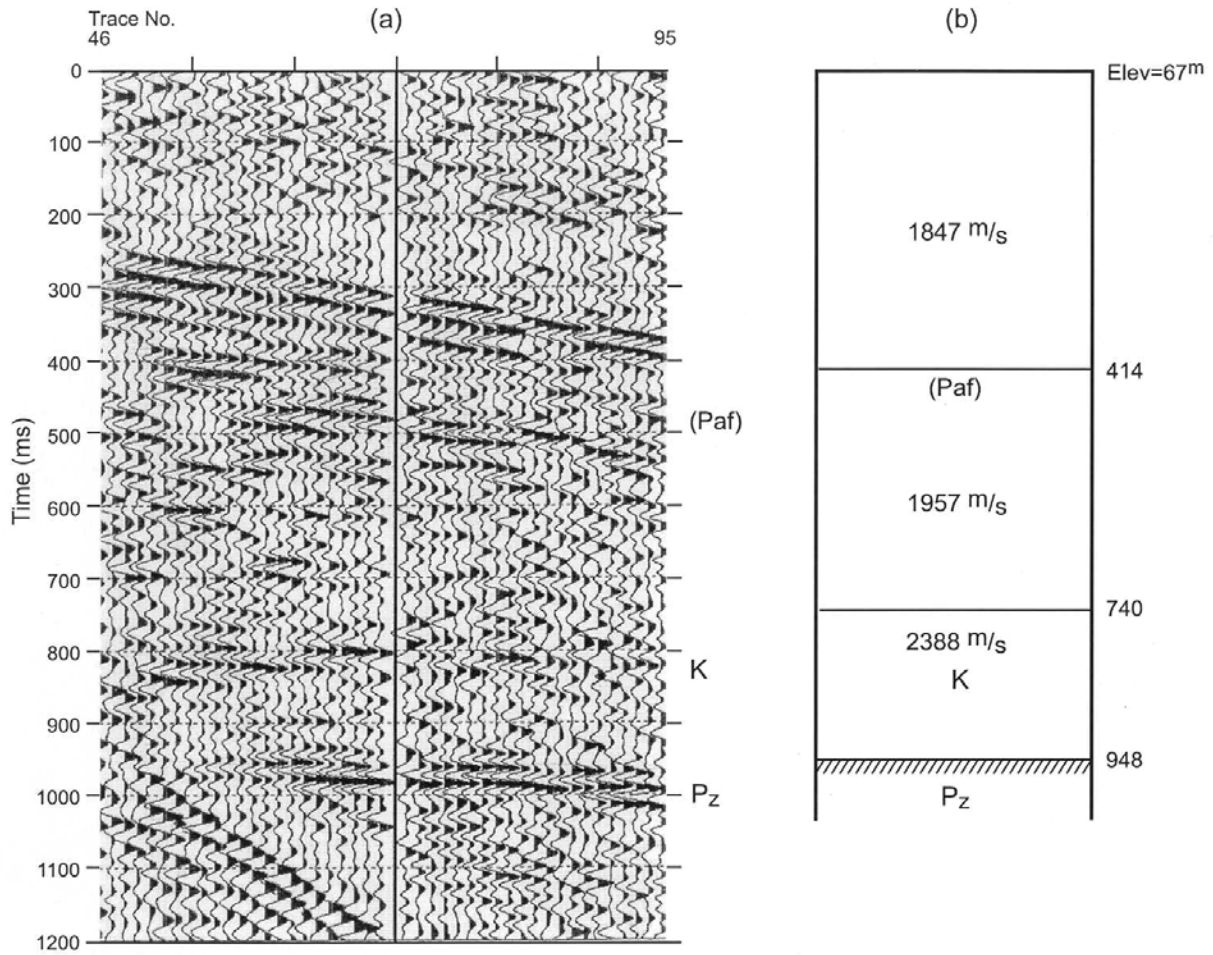
Figure 7. (a) Site 28 P-wave sounding panel and (b) corresponding velocities interpreted for the site. The P-wave velocity from the surface to a depth of 414 m is the RMS velocity of the sediments, whereas the P-wave velocities from 414 to 740 and 740 to 948 are interval velocities.

24
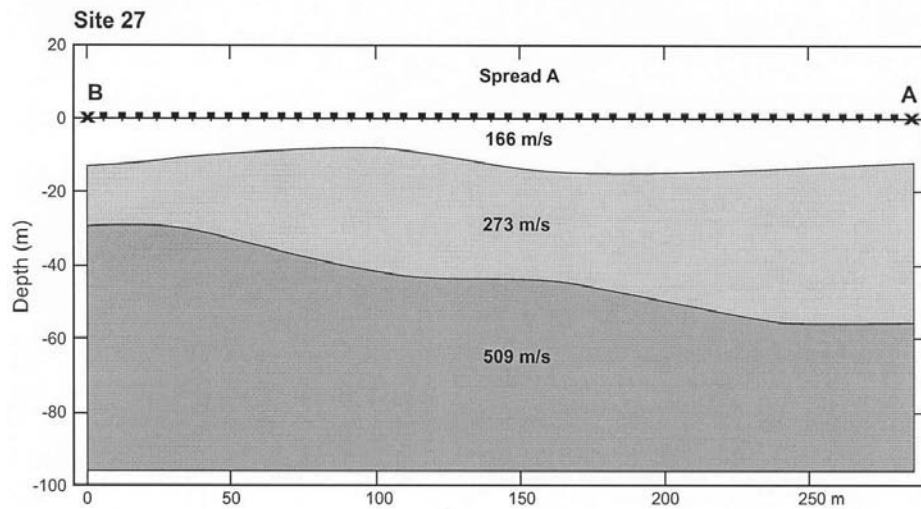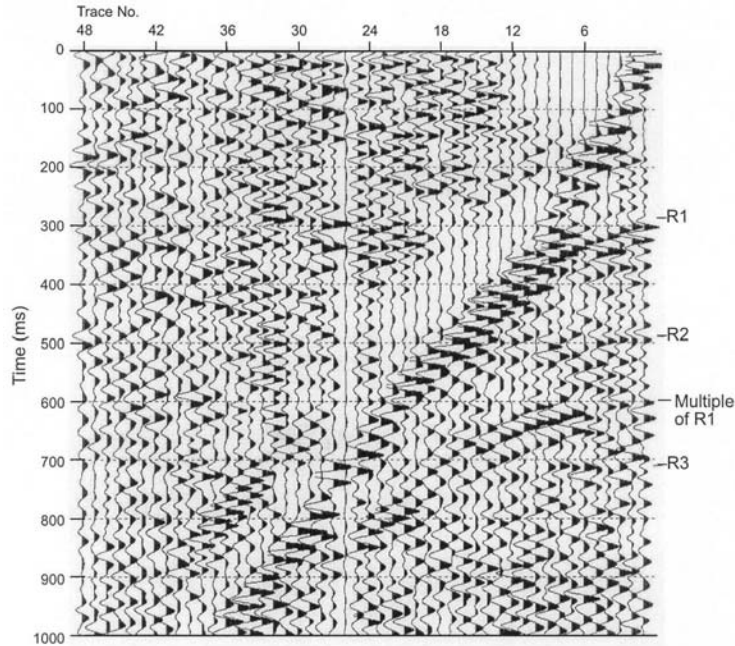
Figure 8. (a) One side of the reversed SH-wave profile acquired at site 28, and the three identified reflectors, R1, R2, and R3 (shown along the right side of the record section). (b) The S-wave velocity refraction model for site 28 based on the first arrivals in the reversed SH-wave seismic profiles, and evaluated using the SIP (Rimrock Geophysics, Inc., 1995) software.

25
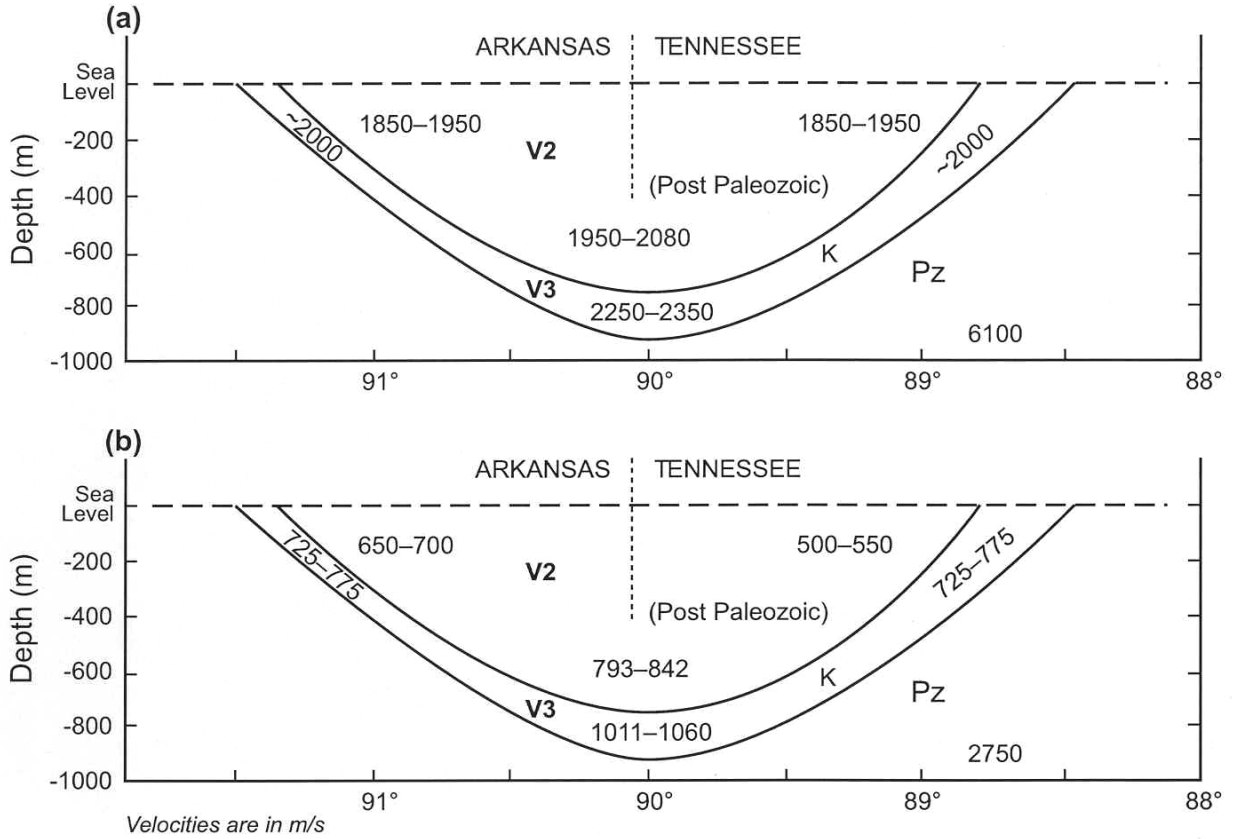
Figure 9. (a) P-wave velocities and (b) S-wave velocities for the post-Paleozoic sediments between latitudes 35¼ and 35½° N that are deeper than 100 m (note vertical exaggeration). Velocities were found to vary both vertically and laterally. The bedrock S- and P-wave velocities are from Dorman and Smalley (1994).
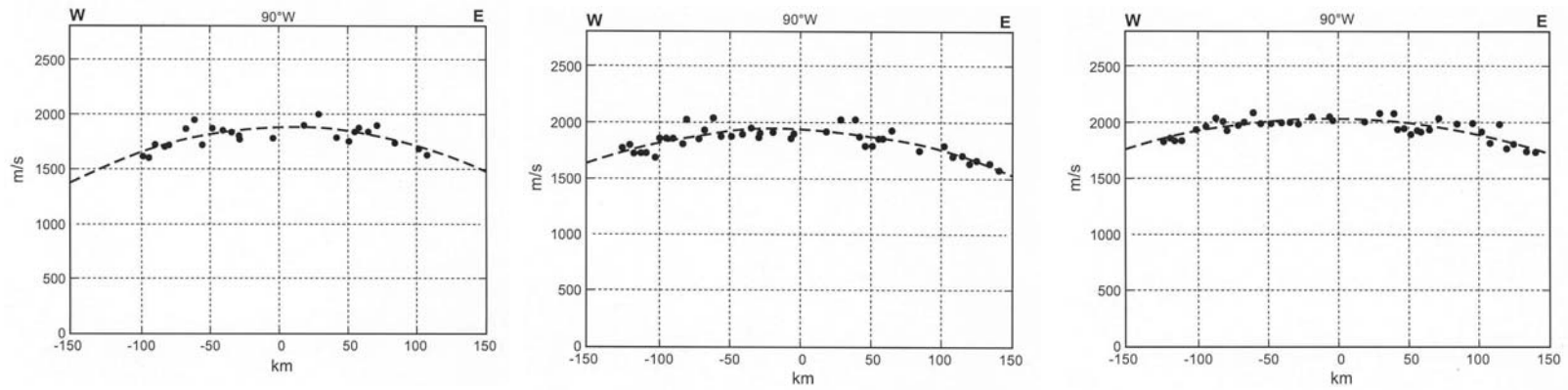
Figure 10. Plots showing P-wave RMS velocities (filled circles) to (a) the top of the Fort Pillow Formation, (b) the top of the Cretaceous section, and (c) the top of the Paleozoic bedrock. Dashed lines superimposed on the plots are a least-squares data fit.
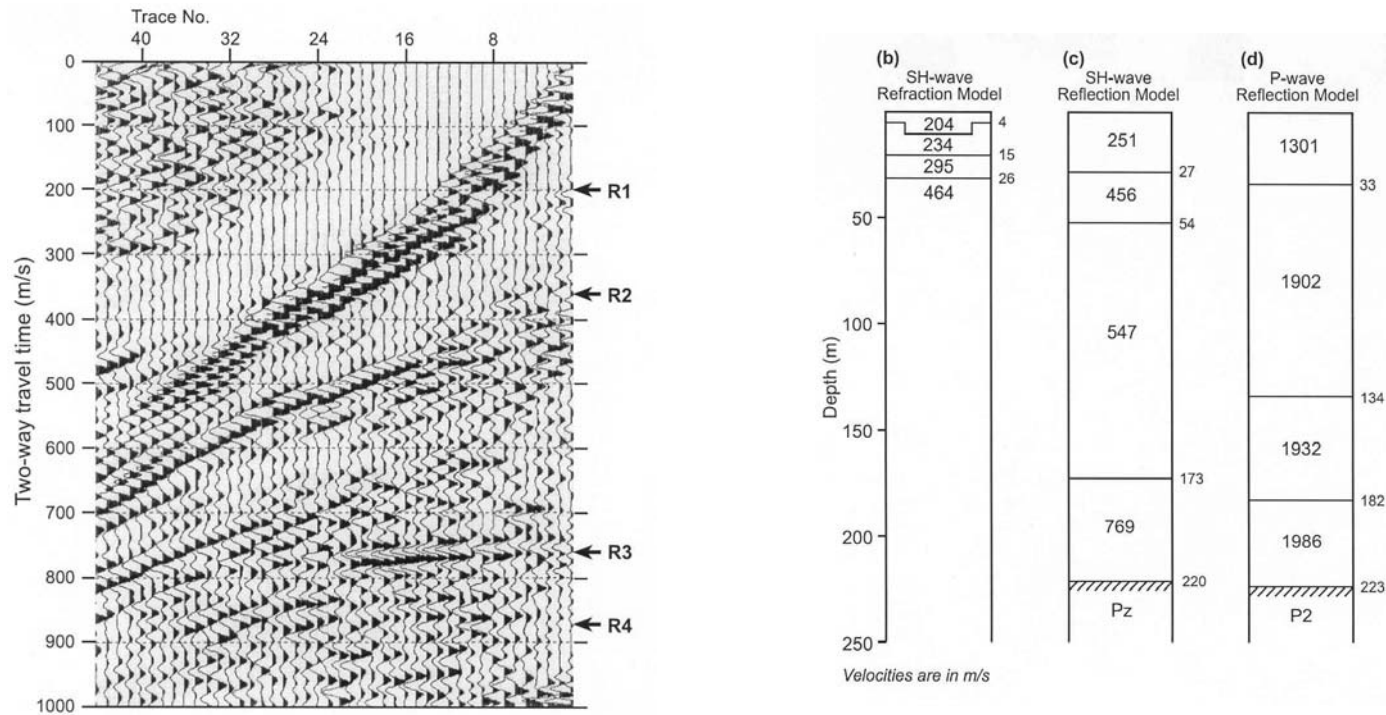
Figure 11.  (a) One side of the reversed SH-wave seismic data collected at site 10 that show the reflections used in determining the S-wave velocities at the site.  A comparison of the S- and P-wave velocity models for site 10 based on (b) refraction modeling of the reversed SH-wave seismic data, and (c) the estimation of the RMS and (d) interval velocities from the SH- and P-wave (not shown) seismic data at the site.  In general, the refraction modeling provides the most detailed information on the near-surface velocities and is the best method for detecting near-surface velocity structures, whereas the reflection data provide the best depth of penetration.  The use of all three data sets, along with the depth to bedrock based on the available drillhole data, provides for a rigorous check of the model accuracy.

### (a)

| Seismic Station | TWAR | BLAR | NFAR |
|---|---|---|---|
| H(m) | 917 | 965 | 915 |
| $dt_{S-Sp}$ (s) | 0.82±0.04 | 0.83±0.04 | 0.82±0.04 |
| $V_p$(m/s) | 2,008 | 2,008 | 2,008 |
| $V_s$(m/s) | 696–742 | 715–759 | 695–740 |
| T(s) | 1.317–1.235 | 1.351–1.271 | 1.318–1.236 |
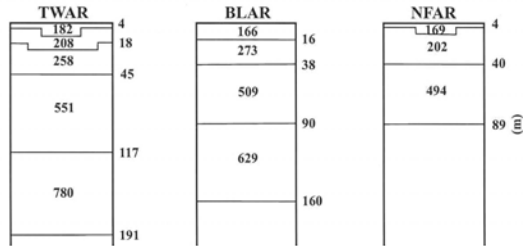
### (c)

| Seismic Station | TWAR | BLAR | NFAR |
|---|---|---|---|
| dt(s) | 0.419 | 0.390 | 0.301 |
| T–dt (s) | 0.816–0.898 | 0.881–0.961 | 0.935–1.017 |
| H–h (m) | 726 | 805 | 826 |
| $K^T$ (m) | 190 | 200 | 190 |
| layer 2: $V_s$ (m/s) | 761–842 | 793–868 | 771–842 |
| layer 3: $V_s$ (m/s) | 979–1060 | 1011–1086 | 989–1,060 |
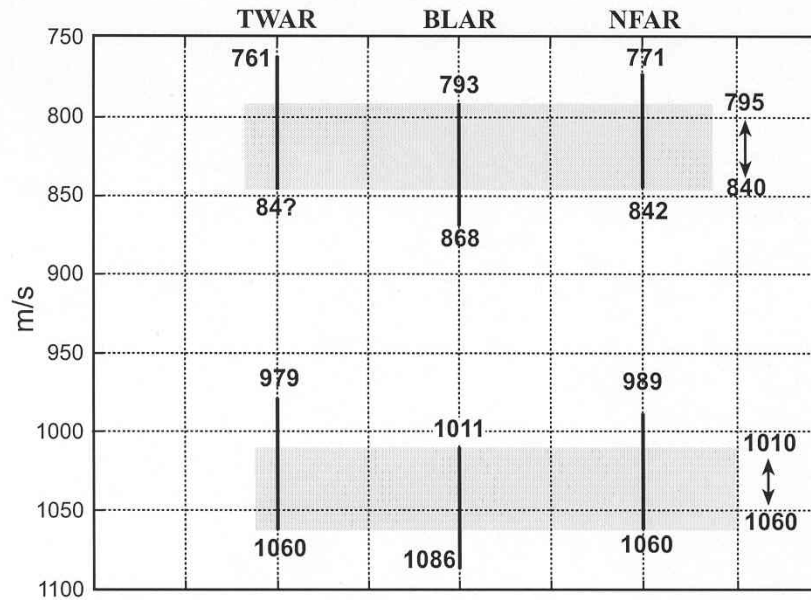
Figure 12. Procedure outline for estimating the S-wave velocities of the post-Paleozoic sediments at the seismograph stations TWAR, BLAR, and NFAR. In part (a), H(m) is the thickness of the sediments at the stations; $dt_{S-Sp}$(s) is the difference in the travel times between the S- and S$p$-waves at the stations as observed on seismograms of earthquakes; $V_p$ (m/s) is the P-wave velocity at the sites based on averaged velocities shown in Figure 10c; $V_s$ (m/s) is the range of S-wave velocities at the stations based on equation (1) and the standard deviation of 0.04 (s) suggested for $dt_{S-Sp}$(s). Part (b) shows the S-wave velocity models developed for the three seismic stations from the seismic reflection/refraction data. Part (c) gives the one-way travel times (dt) through the near-surface velocity layers shown in part b; the one-way travel times (T-dt) for a S-wave traveling vertically through the sediments; the total thickness of the sediments minus the thickness of the near-surface sediments in part b (i.e., H-h), and the thickness of the Upper Cretaceous layer at the seismic stations based on the P-wave soundings. The ranges of the S-wave velocities estimated for layer 2 and layer 3 (i.e., the Cretaceous) are shown in the bottom part of the table. The underlined values indicate the minimum and maximum values that satisfy all three stations simultaneously. Part d of the figure shows the ranges of S-wave velocities estimated for the two layers at each of the three seismic stations, and the ranges of permissible values. The values have been rounded off to the nearest 5 m/s increment.
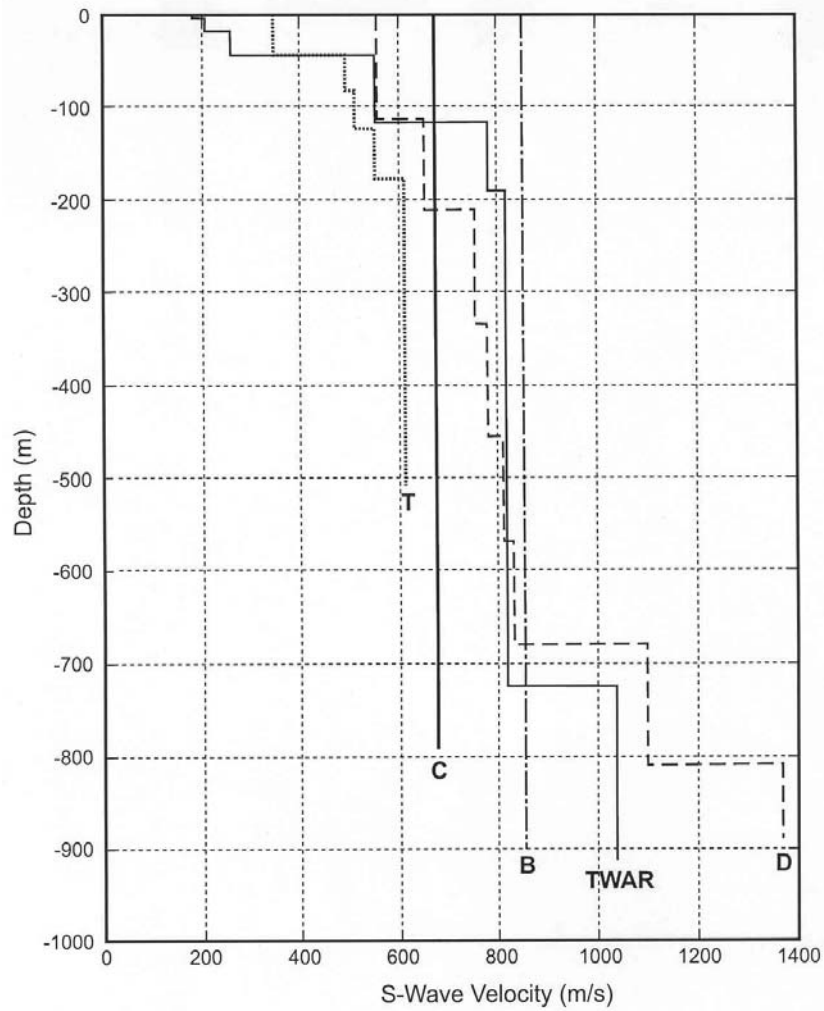
Figure 13. A comparison of the S-wave velocity models by Chiu et al. (1992), Toro et al. (1992), Dorman and Smalley (1994), and Bodin and Horton (1999) to that derived in this study at seismic station TWAR. Velocity models are labeled C for Chiu et al., T for Toro et al., B for Bodin and Horton, and D for Dorman and Smalley (1994).
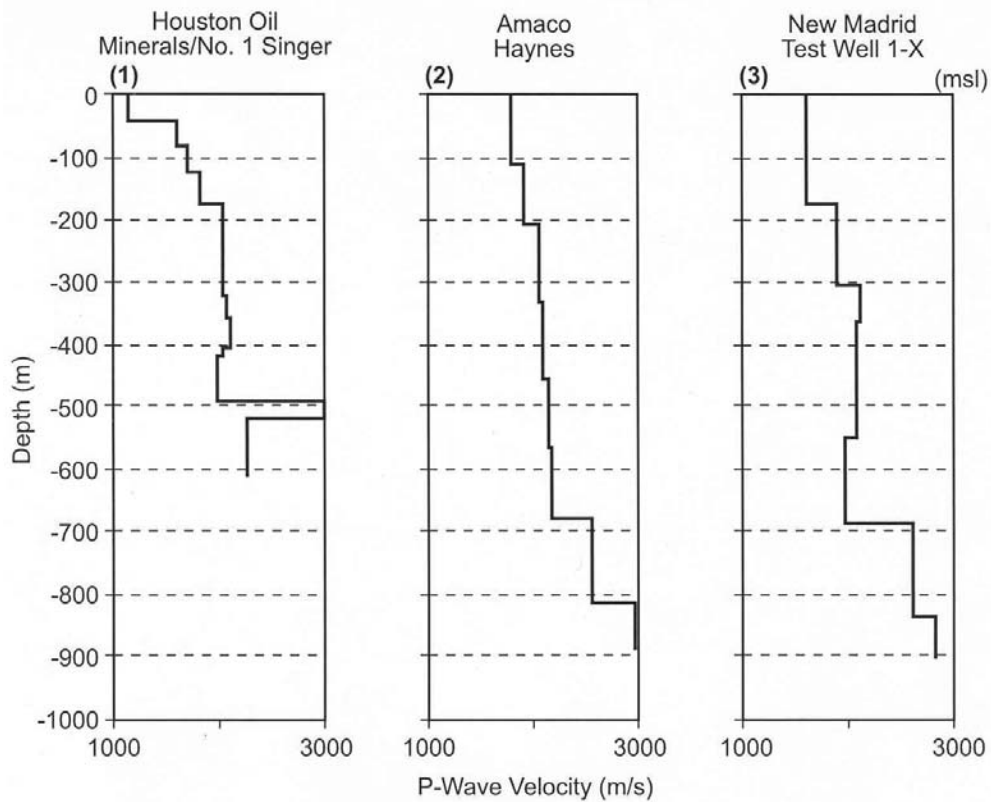
Figure 14. A comparison of P-wave velocity models derived from sonic logs at the three drillholes whose locations are shown in Figure 1.